SAND2013-10354C

PAH Formation and Soot Morphology in Flames of C_4 Fuels

M. Schenk,[1*] *N. Hansen,*[2*] *H. Vieker,*[3] *A. Beyer,*[3] *A. Gölzhäuser,*[3] *K. Kohse-Höinghaus*[1]

[1]Department of Chemistry, Bielefeld University, D-33615 Bielefeld, Germany

[2]Combustion Research Facility, Sandia National Laboratories, Livermore, CA 94551, USA

[3]Department of Physics, Bielefeld University, D-33615 Bielefeld, Germany

to be submitted to:

35th International Symposium on Combustion

"Soot, PAH and other large molecules" Colloquium

Word Count (MS Word)

Abstract:	202
Introduction:	358
Experimental Procedures:	488
Results and Discussion:	1727
Conclusions:	183
Acknowledgements:	45
38 References:	699
2 Tables: 68+61	129
5 Figures: 156+148+385+524+315+640	2168
Total Words (excluding abstract):	**5797**

[*] Corresponding authors: nhansen@sandia.gov, +1 925-294-6272 (NH), marina.schenk@uni-bielefeld.de, +49 521-106-6308 (MS)

Abstract

In this work, we describe experimental studies on the formation of polycyclic aromatic hydrocarbons (PAH's) in opposed-flow atmospheric-pressure flames of *n*-butane, *i*-butane, *i*-butene, and *i*-butanol and on the morphology of nascent soot particles sampled from premixed atmospheric-pressure flames of the same fuels. To identify the major contributors to the molecular growth mechanism in the opposed-flow flames, we employed flame-sampling molecular-beam mass spectrometry with electron ionization (EI) and *in-situ* gas-chromatography (GC) with mass spectrometric detection. The EI- and GC-EI mass spectra indicate that several pathways with different building blocks can contribute to molecular growth. Besides the commonly accepted hydrogen-abstraction-C_2H_2-addition steps, we found reactions of the methyl radical to be important steps. This observation is also supported by the complexity of the mass spectra which indicates that at least one of the building blocks is rather small. The importance of phenyl radicals as building blocks seems to be limited. We also used helium-ion microscopy to unravel the influence of the fuel structure on the morphology of nascent soot particles and we found that the observed differences in shape and size of the sampled soot particles are a likely due to a combined effect of temperature, residence time, and chemical nature of the fuel.

Introduction:

Understanding the chemical details of the soot formation processes in flames remains an intriguing problem in combustion chemistry research and significant progress has been made over the last few years. It is now believed that polycyclic aromatic hydrocarbons (PAH's) are the molecular precursors of soot particles [1, 2]. It is also accepted that the overall soot-forming chemistry starts with the formation of the so-called "first aromatic ring" with its formation dominated by reactions of resonantly stabilized radicals like propargyl, allyl, *i*-C_4H_5, and C_5H_5 [3-5]. The following molecular growth of the PAH's from benzene is generally described as a repetitive reaction sequence of a hydrogen abstraction followed by acetylene (C_2H_2) addition [6, 7], but new experimental results and theoretical considerations throw doubt on the general validity of this so-called HACA mechanism [1, 2, 8, 9]. To develop a better understanding of the PAH growth chemistry, new experimental insights are necessary in order to guide the development and optimization of a validated and predictive combustion modeling capability.

In this paper, we present new experimental insights with regards to the soot formation chemistry in laboratory-scale opposed-flow and premixed model flames fueled by the C_4 species *n*-butane, *i*-butane, *i*-butene, and *i*-butanol. The opposed-flow flames were analyzed with flame-sampling molecular-beam mass spectrometry employing electron ionization including isomeric separation of the PAH's based on gas chromatography [10]. Furthermore, we show helium-ion microscopy (HIM) images of nascent soot particles from laminar premixed atmospheric-pressure flames of the same fuels. The HIM technique [11, 12] allows for additional insights to the morphology of soot particles [13].

The purpose of this investigation is to obtain more experimental insights into the chemistry of soot formation and to provide benchmarks for flame chemistry model development

with regards to PAH growth. Keeping in mind that recent advances in combustion chemistry modeling have led to a detailed understanding of the small molecule chemistry in flames of these C_4 fuels [10, 14-16], we have shifted the focus of this work on the larger molecular species containing up to four condensed aromatic rings (pyrene). We also discuss the impact of the fuel structures on the morphology of the nascent soot particles [13, 17-19].

Experimental Procedures:

Gas-Phase Experiments:

Flame-sampling molecular-beam mass spectrometry (MBMS) has been established at Bielefeld University as a sophisticated tool to analyze laboratory-scale model flames. The general concepts of this technique have been described previously [10, 14, 20] and only a few details are provided here. The used spectrometer consists of a two-stage Wiley-McLaren ion source with soft ionization using energetic electrons. The resulting molecular ions are separated in a reflectron time-of-flight unit which provides a mass resolution of $m/\Delta m \sim 2500$ and subsequently the ions are detected using a multi-channel plate with a multi-channel scaler for data recording.

For this study, the typically used flat-flame burner was replaced with a home-built opposed-flow atmospheric-pressure flame system [21] and the gases were sampled via a microprobe with a ~20 μm orifice, similar to the experiments described by Skeen *et al.* [9, 22]. The non-premixed (diffusion) flames of this study offer the advantage that they can potentially produce PAH's in higher concentration compared to the premixed flames. The conditions for the opposed-flow atmospheric-pressure flames of *n*-butane, *i*-butane, *i*-butene, and *i*-butanol are given in Table 1.

To provide isomer-specific information for stable intermediates, which are not available from MBMS with electron ionization (EI) alone, we also performed probe-sampling *in-situ* gas chromatography (GC) and mass spectrometry experiments according to the procedures described in Ref. [10]. We have utilized a low polarity column (Restek, Rxi-5Sil MS) in order to separate the commonly expected PAH's intermediates. A GC program suitable for the separation of large hydrocarbons was applied, from 50°C (10 min hold) to 300°C (heating rate 25°C/min, 15 min hold, total duration 35 minutes). The identification was made with the use of reference chromatograms obtained from the supplier [23, 24] and by the use of reference substances whenever feasible.

Helium-ion microscopy:

In addition to the gas-phase experiments, we used helium-ion microscopy (HIM) [12] to gain additional insights to the morphology of soot particles, which we sampled from atmospheric-pressure burner-stabilized flames of the above mentioned C_4 fuels [13, 25, 26]. For these experiments, sooting flames ($\phi = 2.04$, for flame conditions see Table 2) were stabilized on a water-cooled, atmospheric-pressure porous plug burner and the soot particles were probed at two different heights, applying the thermophoretic sampling technique [26]. A silicon wafer (area ~1 cm^2) was mounted on a stepper motor and moved through the flame at the different heights. HIM is a scanning microscopy method, where a fine beam of helium ions is scanned pixel-by-pixel over a sample surface. It features a sub-nm resolution due to a small spot size (0.25 nm) and localized beam–sample interaction. Additional advantages are the high source brightness and low sample damage [11, 27]. The experiments in this work were conducted with a Carl Zeiss Orion Plus instrument. The working distance was held between 9.2 and 10.1 mm,

while a beam current of up to 0.9 pA was applied. Secondary electrons were detected by an Everhart–Thornley detector.

Results and Discussion:

A typical result of the flame-sampling EI-MBMS experiments is shown in Fig. 1 for the mass range of *m/z*=75-210. This data were taken from within the *i*-butene flame near the sooting region. Similar looking mass spectra were obtained when sampling from within the other flames. As can be seen, the mass spectrum is quite crowded and it is obviously beyond the scope of the present paper to present detailed information in the form of quantitative isomeric composition for all of these intermediates. Quantitative mole fraction profiles and modeling results will be presented in a future paper and only a few highlights from the different mass spectra are presented here.

Furthermore, it is important to note that the resolution of the mass spectrometer is not sufficient to separate polycyclic aromatic hydrocarbons from oxygenated near-mass species. This limitation precludes the identification of large oxygenated species, maybe anticipated to be present in the *i*-butanol flame, and for the following discussion we therefore assume that all observed mass peaks are due to the hydrocarbon species.

It is obvious from the complexity of the observed mass spectra that multiple pathways of more than one building block must be responsible for the molecular growth of the PAH molecules. This result is not surprising, considering the fact that multiple pathways can already contribute to the formation of the first aromatic ring, *i.e.* benzene [5, 28]. Furthermore, the crowded mass spectra also indicate that at least one of the molecular building blocks must be rather small.

Besides the widely spread HACA mechanism several other pathways have been discussed in the recent literature describing the role of phenyl and methyl radicals [29-32]. Evidence for the molecular growth through methyl radicals is found in the sequences of mass peaks at repeating intervals of 14 amu (+CH_3/-H). For example, such a sequence starts from benzene (*m/z*=78) with the corresponding peaks of that sequence at *m/z*=92, 106, 120. Similar sequences can be found starting from indene (*m/z*=116) or naphthalene (*m/z*=128). Examples of the respective species profiles are shown in Fig. 2 for the sequences starting at *m/z*=78 and 128. As can be seen, the sequences normally come to a stop after the addition of three or less methyl groups, thus maybe indicating a limited importance of this growth mechanism. However, Shukla *et al.* argue that in their pyrolysis experiments the most likely isomers on *m/z*=106 and 156 are the ethyl-substituted benzene or naphthalene rings rather than the dimethyl-substituted isomers [32]. Such an assignment would help to explain the prominent peaks at *m/z*=104 and 154, with the isomers styrene and vinyl-naphthalene (or acenaphthene) formed via dehydrogenation (or dehydrocyclization) from *m/z*=106 and 156, respectively. These conceivable routes are graphically summarized in Fig. 3. However, it seems rather unlikely that the second methyl addition happens only at the methyl-side rather than on the ring to form the di-methyl substituted isomer. Furthermore, it is worth mentioning that only the route via the 1-methyl- and 1-ethyl-naphthalene (*m/z*=142 and 156) could lead to the acenaphthylene, but that the similar 2-substituted isomers would react differently.

Results from the GC-experiments indicate that signal at *m/z*=128, 142, and 152 can be assigned to contributions from naphthalene, methyl-naphthalene, and acenaphthylene. Examples of the GC-MS results are shown in Fig. 4 and it can be seen that for all four flames similar chromatograms were obtained. The signal of *m/z*=142 (methylnaphthalene) was evaluated from

the *i*-butene flame, but only very small contributions were observed in the *n*- and *i*-butane flames. Possibly because of the lower overall PAH concentration in the *i*-butanol flame [14, 33], the isomers with *m/z*=142 and 152 could not be detected. Besides identifying naphthalene, methylnaphthalene, and acenaphthylene based on their elution time and mass-to-charge ratio, toluene, styrene, and indene were positively identified as main contributors to *m/z*=92, 104, and 116 [23, 24].

No isomer-identifying GC-data exist for *m/z*=154 and 156, but the isomers depicted in Fig. 3 seem plausible and could potentially explain the formation of the $C_{12}H_8$ isomers at *m/z*=152.

With regards to Fig. 3, we would like to discuss two more important aspects. In addition to the shown $C_{12}H_{10}$ isomers, it seems fair to assume that biphenyl contributes to the signal at *m/z*=154. However, the relatively low intensity of this peak would indicate only a limited importance of the phenyl radical as a building block for PAH formation under the experimental conditions of this study. This conclusion is also supported by the fact that in the GC-MS experiments biphenylene was not detected at *m/z*=152 and, as mentioned above, by the complexity of the mass spectra. However, concentrations of biphenyl may also be low because of its fast reactions with methyl or acetylene to form fluorene ($C_{13}H_{10}$, *m/z*=166) or phenanthrene ($C_{14}H_{10}$, *m/z*=178), both of which have been identified in the GC-MS experiments. Second, acenaphthylene (*m/z*=152), which was also identified in the GC-MS experiments, can be formed more efficiently through the HACA mechanism directly from naphthalene. This fact may again explain the relative height of the peak at *m/z*=152. Also, it has been established now that the H-abstraction-acetylene addition mechanism provides a facile route to five- and six-membered ring species via the sequences naphthalene → acenaphthylene → cylopenta[fg]acenaphthylene and

biphenyl → phenanthrene → pyrene [6, 34, 35]. Both these sequences are seen in our flame-sampled mass spectra and are also (at least partly) shown in Fig. 3.

The last reaction pathways to be discussed here are ring-enlargement reactions. It has been well established that fulvene can undergo a hydrogen-assisted isomerization reaction to form benzene [5, 36, 37]. Similar reactions seem conceivable for multi-ring structures and although these experimental results to do not provide direct evidence, these reactions should be tested in flame chemistry modeling of PAH growth. For example, the GC-experiments confirmed the presence of five-membered ring-structures at *m/z*=116 (indene), 152 (acenaphthylene), and 166 (fluorene). See Fig. 5 for more details. These species represent the main two types of five-membered ring structures in PAH's, the one with a saturated CH_2 group (indene and fluorene) and the unsaturated one with only CH groups (acenaphthylene). An even more saturated ring (like in indane, *m/z*=118) seems plausible but no experimental confirmation can be provided here. Please note that the saturated CH_2 group in indene and fluorene disturbs to some extent the resonance stabilization and that the respective radicals (with an H removed from the CH_2 group) are entirely resonantly stabilized, thus very stable, structures. This fact seems to be responsible for the larger signal of these radicals (with respect to the neutral molecule) compared to the radicals (and neutral molecules) at *m/z*=127(128), 151(152), and 177(178).

Figure 5 also indicates the presence of combustion intermediates with *m/z*=130, which could potentially be formed via methyl-addition/H-loss from indene (*m/z*=116), as well as the dehydrogenation step ending in the very stable naphthalene. A similar sequence starting at fluorene and ending at phenanthrene is shown as well. The unsaturated acenaphthylene reacts differently upon methyl addition to the five-membered ring and forms the unsaturated six-membered ring structure 1H-phenalene, another $C_{13}H_{10}$ isomer at *m/z*=166 (besides fluorene).

In general, the mass spectra seem to indicate that multiple pathways contribute to PAH formation in the flames of the four different C_4 fuels and detailed modelling work is necessary to fully understand the flame-sampled mass spectra of the PAH's. Because the chemical growth mechanism will eventually lead from gas-phase molecules to nascent soot particles, we found it interesting to also compare the morphology of such nascent particles when sampled from flames of the studied fuels. To this end, we employ helium-ion microscopy, recently shown to be an excellent tool for soot morphology studies [13].

A series of representative helium-ion micrographs for nascent soot particles probed at two different heights from a burner-stabilized premixed *n*-butane flame and an *i*-butanol flame is shown in Fig. 6. An overview of particles probed from the four flames is shown in Fig. S1-S4 of the Supplemental Material. For the soot sample probed at 0.8 cm distance from the burner surface of the *n*-butane flame, small particles (circles, pentagons) of around 8 nm diameter are visible, and some smaller particles start to grow into aggregates (rectangles). The instrument can detect particles smaller than 5 nm. For the particles probed at 1.2 cm above the burner surface, the aggregates have grown into larger structures, while the small particles are still detectable. The overall contrast of the soot particles to the silicon substrate is very good. For the soot sample collected in the *i*-butanol flame at 0.8 and 1.2 cm, the contrast of the particles to the substrate is less pronounced, and the small particles probed at 0.8 cm are in the range of below 8 nm in diameter. At 1.2 cm height, the particles have larger diameters and are most probably aggregates that are formed from smaller particles, but their outer shape is less distinguished compared to the aggregates probed from the *n*-butane flame, instead they show a more elliptical or spherical shape. Camacho *et al.* [19],who have recently studied slightly sootier flames of the *n*- and *i*-isomers of butane and butanol in terms of impact of the fuel-bound oxygen on soot formation,

reported that the maximum temperature of the burner-stabilized *n*-butane flame (1750 K±70 K) is slightly lower compared to the temperature in an *i*-butanol flame with the same C/O ratio (1790±50 K), the same holds for the adiabatic flame temperature of the flames. With this, the different morphology of the soot particles from the two flames can be explained by three aspects. On the one hand, the difference in temperature might account for the different morphology of the particles, as the particle/aggregate sizes tend to be smaller for higher temperatures. On the other hand, the cold gas velocity is slightly higher for the *i*-butanol flame (see Table 2), which directly correlates with the residence time, and the particles might be smaller as the reaction time is shorter. As a third possible explanation of the different morphology, the chemical differences may come into play. For example, Alfé *et al.* [38] have investigated the difference between soots collected from flames of CH_4, C_2H_4, benzene, and cyclohexane, and they have found a strong correlation between the nature of the fuel and the resulting nanostructure of the particles. It is likely that that the different organization of the soot particles in this study results from the combined effects of temperature, residence time, and chemical nature of the fuel.

Conclusions:

PAH growth and soot formation remain an intriguing problem in combustion chemistry research. In this study we have provided experimental evidence in the form of flame-sampling GC-EI-MS and EI-MBMS that multiple pathways contribute to the PAH formation in the flames of the C_4 fuels *n*-butane, *i*-butane, *i*-butene, and *i*-butanol. Independent of the fuel-structure, the same building blocks seem to be responsible for the PAH growth chemistry in the different flames. Sequences in the mass spectra were observed which can result from the well accepted HACA mechanism and from various CH_3 growth reactions, including C_5-C_6 ring-enlargement

reactions. Methyl-substituted PAH's seem to be major intermediates and the importance of a small building block for PAH growth is also highlighted by the fact that the flame-sampled mass spectra are very complex. We find the different organizations of the nascent soot particles from within the different flames very intriguing and the observed differences in the morphology of the sampled particles are likely the result of a combination of temperature, residence time, and chemical nature of the fuel. More detailed studies are necessary to unravel these effects.

Acknowledgements:

The authors thank H. Waterbör for expert technical assistance. NH was in part supported by the Division of Chemical Sciences, Geosciences and Biosciences, Office of Basic Energy Sciences, U.S. Department of Energy under contract DE-AC04-94-AL85000. NH also acknowledges funding through the Alexander von Humboldt-Foundation.

References:

[1] H. Bockhorn, A. D'Anna, A.F. Sarofim, H. Wang (Eds.), Combustion generated fine carbonaceous particles, KIT Scientific Publishing, Karlsruhe, 2009.

[2] H. Wang, Proc. Combust. Inst. 33 (2011) 41-67.

[3] C. S. McEnally, L. D. Pfefferle, B. Atakan, K. Kohse-Höinghaus, Progr. Energy Combust. Sci. 32 (3) (2006) 247-294.

[4] J. A. Miller, M. J. Pilling, J. Troe, Proc. Combust. Inst. 30 (2005) 43-88.

[5] N. Hansen, J. A. Miller, S. J. Klippenstein, P. R. Westmoreland, K. Kohse-Höinghaus, Combust. Expl. Shock 48 (5) (2012) 508-515.

[6] M. Frenklach, Phys. Chem. Chem. Phys. 4 (11) (2002) 2028-2037.

[7] M. Balthasar, M. Frenklach, Proc. Combust. Inst. 30 (2005) 1467-1475.

[8] A. Keller, R. Kovacs, K. H. Homann, Phys. Chem. Chem. Phys. 2 (8) (2000) 1667-1675.

[9] S. A. Skeen, H. A. Michelsen, K. R. Wilson, D. M. Popolan, A. Violi, N. Hansen, J. Aerosol Sci. 58 (2013) 86-102.

[10] M. Schenk, L. Leon, K. Moshammer, P. Oßwald, T. Zeuch, L. Seidel, F. Mauss, K. Kohse-Höinghaus, Combust. Flame 160 (3) (2013) 487-503.

[11] D.C. Bell, Microsc. Microanal. 15 (2009) 147-153.

[12] B.W. Ward, J.A. Notte, N.P. Economou, J. Vac. Sci. Technol. B 24 (2006) 2871-2874.

[13] M. Schenk, S. Lieb, H. Vieker, A. Beyer, A. Golzhauser, H. Wang, K. Kohse-Höinghaus, Chemphyschem 14 (14) (2013) 3248-3254.

[14] P. Oßwald, K. Kohse-Höinghaus, U. Struckmeier, T. Zeuch, L. Seidel, L. Leon, F. Mauss, Z. Phys. Chem. 225 (9-10) (2011) 1029-1054.

[15] N. Hansen, S. S. Merchant, M. R. Harper, W. H. Green, Combust. Flame 160 (11) (2013) 2343-2351.

[16] S. M. Sarathy, S. Vranckx, K. Yasunaga, M. Mehl, P. Oßwald, W. K. Metcalfe, C. K. Westbrook, W. J. Pitz, K. Kohse-Höinghaus, R. X. Fernandes, H. J. Curran, Combust. Flame 159 (6) (2012) 2028-2055.

[17] A. C. Barone, A. D'Alessio, A. D'Anna, Combust. Flame 132 (1--2) (2003) 181-187.

[18] C. Russo, M. Alfè, J.-N. Rouzaud, F. Stanzione, A. Tregrossi, A. Ciajolo, Proc. Combust. Inst. 34 (1) (2013) 1885-1892.

[19] J. Camacho, S. Lieb, H. Wang, Proc. Combust. Inst. 34 (1) 1853-1860.

[20] N. Hansen, T. A. Cool, P. R. Westmoreland, K. Kohse-Höinghaus, Prog. Energy Combust. Sci. 35 (2) (2009) 168-191.

[21] A. Brockhinke, A. Bülter, J. C. Rolon, K. Kohse-Höinghaus, Appl. Phys. B 72 (4) (2001) 491-496.

[22] S. A. Skeen, B. Yang, H. A. Michelsen, J. A. Miller, A. Violi, N. Hansen, Proc. Combust. Inst. 34 (2013) 1067-1075.

[23] Restek Corporation, "GC_EV00684" in Restek Searchable Chromatogram Library, http://www.restek.com/images/cgram/gc_ev00684.pdf.

[24] Restek Corporation, "GC_AR1157" in Restek Searchable Chromatogram Library, http://www.restek.com/images/cgram/gc_ar1157.pdf.

[25] A. D. Abid, J. Camacho, D. A. Sheen, H. Wang, Combust. Flame 156 (10) (2009) 1862-1870.

[26] A.D. Abid, N. Heinz, E.D. Tolmachoff, D.J. Phares, C.S. Campbell, H. Wang, Combust. Flame 154 (775-788) (2008).

[27] D. Cohen-Tanugi, N. Yao, J. Appl. Phys. 104 (2008) 63504.

[28] N. Hansen, T. Kasper, B. Yang, T. A. Cool, W. Li, P. R. Westmoreland, P. Osswald, K. Kohse-Höinghaus, Proc. Combust. Inst. 33 (2011) 585-592.

[29] B. Shukla, M. Koshi, Phys. Chem. Chem. Phys. 12 (10) (2010) 2427-2437.

[30] B. Shukla, M. Koshi, Combust. Flame 158 (2) (2011) 369-375.

[31] B. Shukla, M. Koshi, Combust. Flame 159 (12) (2012) 3589-3596.

[32] B. Shukla, A. Miyoshi, M. Koshi, J. Am. Soc. Mass Spectrom. 21 (4) (2010) 534-544.

[33] C. K. Westbrook, W. J. Pitz, H. J. Curran, J. Phys. Chem. A. 110 (2006) 6912-6922.

[34] V. V. Kislov, A. I. Sadovnikov, A. M. Mebel, J. Phys. Chem. A. 117 (23) (2013) 4794-4816.

[35] M. Celnik, A. Raj, R. West, R. Patterson, M. Kraft, Combust. Flame 155 (1-2) (2008) 161-180.

[36] N. Hansen, W. Li, M. E. Law, T. Kasper, P. R. Westmoreland, B. Yang, T. A. Cool, A. Lucassen, Phys. Chem. Chem. Phys. 12 (38) (2010) 12112-12122.

[37] A. W. Jasper, N. Hansen, Proc. Combust. Inst. 34 (2013) 279-287.

[38] M. Alfè, B. Apicella, R. Barbella, J.-N. Rouzaud, A. Tregrossi, A. Ciajolo, Proc. Combust. Inst. 32 (1) 697-704.

Tables:

Table 1: Flame conditions for the opposed-flow atmospheric-pressure flames

Fuel	Fuel Stream			Oxidizer Stream		
	Mole Fractions		Mass Flow	Mole Fractions		Mass Flow
	x_F	x_{Ar}	$\dot{m}$ / g cm^{-2} s^{-1}	x_{O_2}	x_{Ar}	$\dot{m}$ / g cm^{-2} s^{-1}
n-C_4H_{10}	0.06	0.94	3.2×10^{-2}	0.38	0.62	2.9×10^{-2}
i-C_4H_{10}	0.05	0.95	3.5×10^{-2}	0.38	0.62	2.9×10^{-2}
i-C_4H_8	0.04	0.96	3.4×10^{-2}	0.44	0.56	3.0×10^{-2}
i-C_4H_9OH	0.07	0.93	3.6×10^{-2}	0.38	0.62	2.9×10^{-2}

Table 2: Flame conditions for the burner-stabilized atmospheric premixed flames

Fuel	Mole fractions			Equivalence	Cold Gas Velocity
	Fuel	Oxygen	Argon	Ratio ϕ	[cm/s] at 300K
n-C_4H_{10}	0.0959	0.3043	0.5998	2.04	3.593
i-C_4H_{10}	0.0959	0.3043	0.5998	2.04	3.593
i-C_4H_8	0.0959	0.3043	0.5998	2.04	3.593
i-C_4H_9OH	0.0959	0.3043	0.5998	2.04	3.948

Figures:

Figure 1: (145+11=156 words)

Flame-sampled mass spectrum from within the atmospheric-pressure opposed-flow *i*-butene diffusion flame.

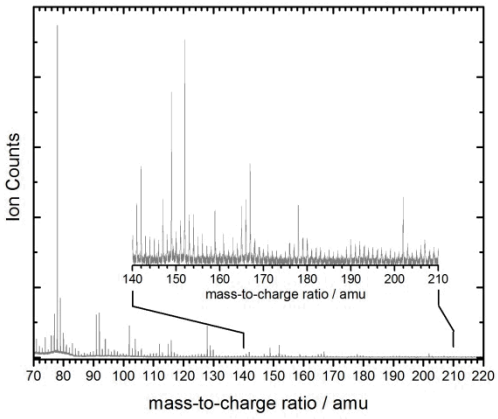

Figure 2: (130+18=148 words)

Species profiles as function of distance from the fuel outlet for methyl-addition sequences starting at *m/z*=78 and 128.

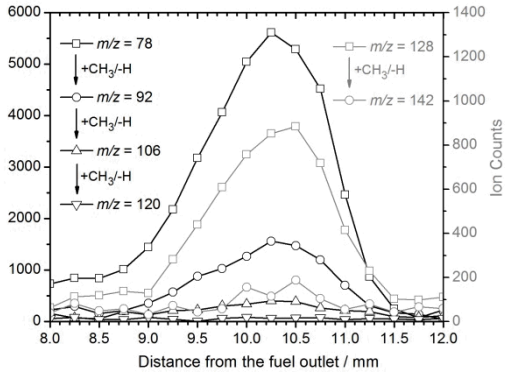

Figure 3: (355+30=385 words)

Mass spectra and conceivable formation pathways of certain isomers. Naphthalene, methyl-naphthalene and acenaphthylene (at *m/z*=128, 142, and 152) have been positively identified using the GC experiments. See text for details.

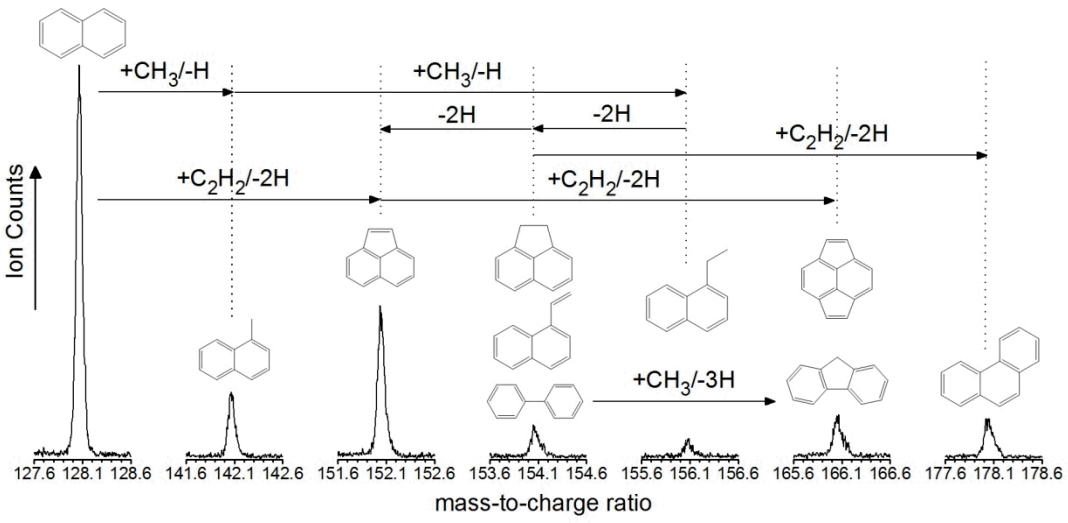

Figure 4: (513+11=524 words)

GC-MS spectra obtained from the flame zones of the four flames.

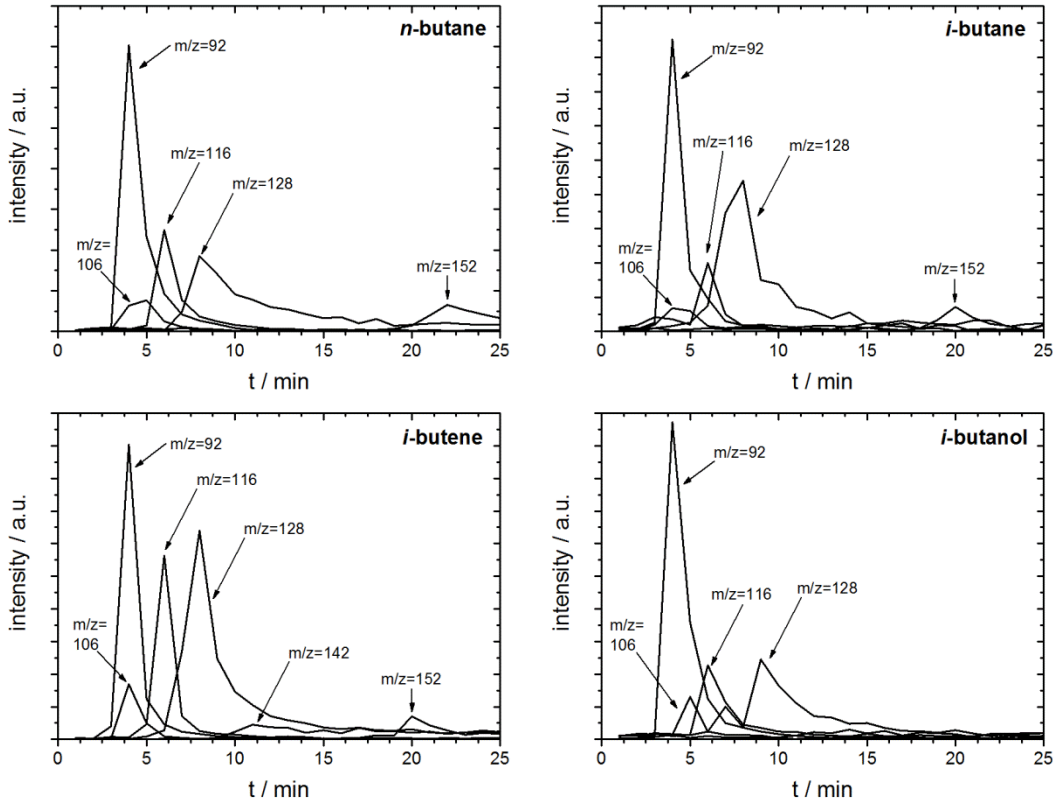

Fig. 5: (290+25=315 words)

Excerpts of a flame-sampled time-of-flight mass spectrum indicating the presence of five-membered ring structures and their possible role in molecular-growth reactions. See text for details.

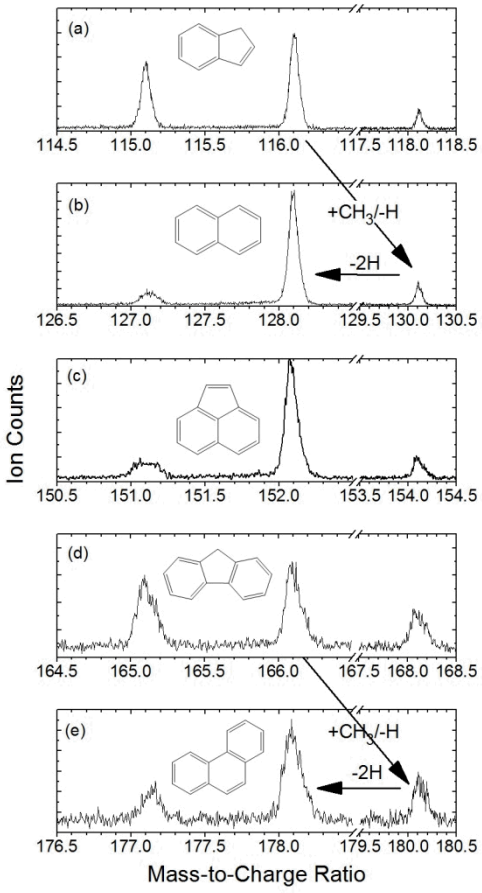

Fig. 6: (615+25 = 640 words)

HIM micrographs for soot probed from atmospheric-pressure flames of *n*-butane (upper row) and *i*-butanol (bottom). For near-spherical particles (circles and pentagons), the diameter is given.